Regular Article

INORGANIC CHEMISTRY RESEARCH
Published by the
Iranian Chemical Society
www.inorgchemres.org
info@inorgchemres.org

***Inorg. Chem. Res.**, Vol. 5, No. 1, 19-36, June 2021*
DOI: 10.22036/icr.2020.235835.1073

Modification of Magnetic TiO_2 Nanocomposite with Co^{III}, Zn^{II} and Ni^{II} Porphyrins for Photodegradation of Methylene Blue under the Blue Vis-LED Light Irradiation

Ensieh Gholamrezapor and Abbas Eslami*

Department of Inorganic Chemistry, Faculty of Chemistry, University of Mazandaran, P. O. Box: 47416-95447, Babolsar, Iran

(Received 19 June 2020, Accepted 11 December 2020)

The magnetic nanocomposites [magnetite@silica@titania@metallo*meso*-tetra(hydroxyphenyl)porphyrin, Fe_3O_4@SiO_2@TiO_2@MTHPP] (MSiTMP; M = Co^{III}, Zn^{II}, Ni^{II}) and [Fe_3O_4@SiO_2@TiO_2] (MSiT) have been synthesized and characterized. These nanocomposites were used to degrade of methylene blue (MB) under the blue light-emitting diode (LED) lamp irradiation. The degradation of MB was monitored by UV-Vis spectrometry. Upon a 180 min irradiation period maximum degradation of MB in presence of MSiTNi^{II}P, MSiTZn^{II}P, MSiTCo^{III}P and MSiT photocatalysts were 90, 80, 63 and 48% g^{-1}, respectively. After three 180 min runs, the photocatalysts still exhibited good activity. From Ultra-Violent-Diffuse reflectance spectroscopy spectra, the band gap energies of the photocatalysts were found to be 2.6, 2.5, 2.4 and 2.2 eV for MSiT, MSiTCo^{III}P, MSiTZn^{II}P and MSiTNi^{II}P, respectively. The results consist with the observed relative photocatalytic activity of the photocatalysts which is as follows: MSiTNi^{II}P > MSiTZn^{II}P > MSiTCo^{III}P > MSiT. The higher photocatalytic properties of MSiTNi^{II}P photocatalyst may be due to the fact that it is more susceptible to receive electron and reach to steady state than that of Zn^{II} and Co^{III} complexes. The degradation of MB using these nanocomposites were found to follow the pseudo first order kinetics.

Keywords: Methylene blue, Metalloporphyrin, Magnetic nanoparticles, Titanium, LED

INTRODUCTION

Nowadays, various pollutants are released into environmental through homelike resources and industrial sewage [1-5]. The recent studies show that semiconductor photocatalysts can be efficient for municipal and industrial wastewater refinery [6]. In this view, the TiO_2 photocatalysts have received great attention because of their potential applications in degradation of pollutants, and their safe, stable, cheap, abundant, and versatile properties [7,8]. The magnetic nanoparticles can be suitable supports for heterogeneous photocatalysts since they can easily be recovered by using a strong magnet. The magnetite (Fe_3O_4) is the most common core material for this purpose that is mainly due to its magnetic property, excellent separation ability, high coercivity and cheap availability [9-12]. Upon direct contact of a photocatalyst such as TiO_2 with the magnetite (Fe_3O_4), the excited electrons of TiO_2 may be transferred to the valence band (VB) of Fe_3O_4. This event would prevent electron transfer to the O_2 molecules, therefore it decreases the activity of photocatalyst for the decomposition of pollutants [12,13]. To overcome this obstacle, a SiO_2 layer is usually placed between TiO_2 and Fe_3O_4, which prevents the undesirable electron transfer from TiO_2 to the naked magnetite [14,15]. The metalloporphyrins were used for photosensitization of TiO_2 based-photocatalyst because they have the vigorous absorption in the range of 500-700 nm (Q bands), and 400-500 nm (Soret band) [16,17]. The porphyrins can be immobilized on the surface of TiO_2, through which enhances the photocatalytic activity of TiO_2 [18,19]. This ability of porphyrin derivatives was employed for photodegradation of various

*Corresponding author. E-mail: eslami@umz.ac.ir

organic pollutants, such as methylene blue [20-22], 4-nitrophenol [23,24], rhodamine B [25] and methyl orange [26]. The earlier reports revealed that the porphyrins which have peripheral hydroxyl groups act as good photosensitizer for TiO_2 [27]. The hydroxyl groups have higher affinity for bonding on TiO_2 than other functional groups. So, four hydroxyl groups on porphyrins may result in stronger bonding with TiO_2 and better catalytic performance than porphyrins with one, two or three hydroxyl groups. In the present study, Co^{III}, Zn^{II} and Ni^{II} complexes of tetra(hydroxyphenyl)porphyrin (MTHPP) have been used as new photosensitizer of TiO_2 for photodegradation of methylene blue (MB). There are several important factors for using visible light-emitting diode (Vis-LEDs) as irradiation sources over other visible light irradiation sources. Heat production and energy consumption in the LED lamps are lower than other types of light sources [28-30]. The generation of heterogeneous photocatalysts with immobilizing transition metal complexes can simplify their use and easy product separation that recycling would be possible [31]. These attractive features of these photocatalysts could help in developing photocatalytic processes for industrial scale in the cleanup of wastewater [32]. In this study, Fe_3O_4 nanoparticles were prepared from the chemical precipitation method and then coated with tetraethoxysilane (TEOS) *via* the sol-gel method. Then, TiO_2 was placed onto $Fe_3O_4@SiO_2$ (MSi) *via* sol-gel method. Finally, Ni^{II}THPP, Zn^{II}THPP and Co^{III}THPP were immobilized on the silica coated magnetic TiO_2 to result in the nanocomposites $Fe_3O_4@SiO_2@TiO_2@$MTHPP (MSiTMP; M = Co^{III}, Zn^{II}, Ni^{II}). The as-prepared MSiTMPs nanocomposites were used as new photocatalyst in the photodegradation of methylene blue (MB) in water under irradiation of blue LED light source.

MATERIAL AND METHODS

Materials

In this work, iron(III) chloride ($FeCl_3.6H_2O$) (270.29 g mol^{-1}), iron(II) chloride ($FeCl_2.4H_2O$) (198.81 g mol^{-1}), titanium tetra isopropoxide (TTIP) $Ti[OCH(CH_3)_2]_4$ (284.22 g mol^{-1}), and tetraethoxysilane (TEOS) ($SiC_8H_{20}O_4$) (208.33 g mol^{-1}) were used for the synthesis of $Fe_3O_4@SiO_2@TiO_2$ (MT) nanocomposites. Furthermore, 4-hydroxybenzaldehyde ($C_7H_6O_2$) (122.12 g mol^{-1}), propionic acid ($C_3H_6O_2$) (74.08 g mol^{-1}), and pyrrole (C_4H_5N) (67.09 g mol^{-1}) were used for the synthesis of porphyrin. All the chemical materials were purchased from Merck Company.

Preparation of Photocatalysts

The magnetic nanocomposite photocatalysts ($Fe_3O_4@SiO_2@TiO_2@$MTHPP) (MSiTMP) (M = Co^{III}, Zn^{II}, Ni^{II}), can be thought of a two stages process in which ($Fe_3O_4@SiO_2@TiO_2$) (MSiT) nanocomposite was prepared first and then it was sensitized with metalloporphyrins

Preparation of ($Fe_3O_4@SiO_2@TiO_2$) (MSiT) Nanocomposite

The Fe_3O_4 (M) was synthesized *via* a chemical precipitation process [33]. A mixture of 30 mmol of $FeCl_3$ and 15 mmol of $FeCl_2$ in 90 ml deionized water was refluxed at 100 °C under inert argon atmosphere (4 h) and the pH of the solution was adjusted to 9 using ammonia solution (25% w/w). Next, the temperature was lowered to room temperature (r.t.), and the precipitate was filtered off and washed by distilled water until the sample pH arrived at natural. The SiO_2 layer was laid on Fe_3O_4 (M) to create $Fe_3O_4@SiO_2$ (MSi) by a sol-gel procedure [6]. For this purpose, 1.0 g prepared M nanoparticles were dispersed in 200 mL ethanol. Then 6 ml ammonia solution (25% w/w) and 2 mL TEOS were separately added. This mixture was stirred for one day at r.t, and the black precipitate (MSi) was separated by an external magnet, it was washed with ethanol several times. It was dried in a vacuum desiccator at r.t for one day. The TiO_2 layer was placed onto MS to make the $Fe_3O_4@SiO_2@TiO_2$ (MSiT) nanocomposite. The TiO_2 shell was provided for coating of TTIP on MSi in a mixture of water and ethanol. At first, solution A was prepared with the mixtures of MSi (1.2 g) and absolute ethanol (25 mL). Then, solution B was prepared with mixtures of TTIP (8 mL) and absolute ethanol (16 mL), and solution C was obtained with the mixtures of the water (850 mL) and absolute ethanol (20 mL). First, solution A was treated under ultrasonic irradiation for 35 min, then was added to solution B. Subsequently, the mixture of solutions A and B was treated under ultrasonic irradiation (35 min). Finally,

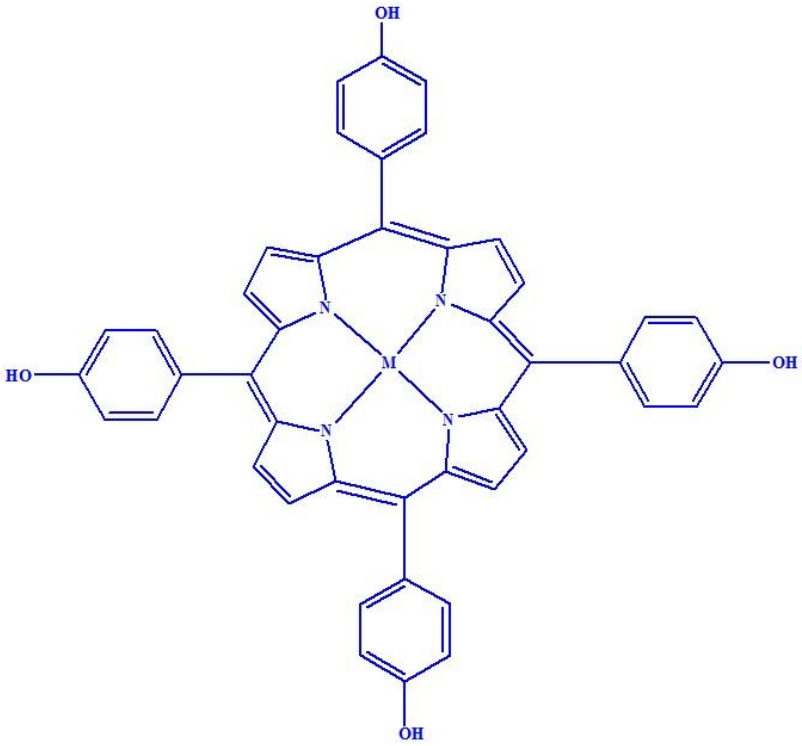

Scheme 1. Chemical structures of MTHPP (M = Co^{III}, Zn^{II}, Ni^{II})

solution C was dropped to the mixture of A and B. Then, the resulted solution was irradiated with ultrasonic waves (1 h). This solution was evaporated in the oven (3 days). Afterward, the obtained nanocomposite was heated at 800 K (2 h). The MSiT nanocomposite was finally washed three times with water to remove impurities. The isolation of the magnetic nanocomposites from aqueous solution was simply performed by a strong magnet.

Preparation of Metallotetrahydroxylphenyl-porphyrin (MTHPP) (M = Co^{III}, Zn^{II}, Ni^{II})

The tetrahydroxylphenylporphyrin (THPP) was prepared according to the literature procedure [34]. For this purpose, 7.46 mmol 4-hydroxybenzaldehyde and fresh distilled pyrrole in 35 mL glacial acetic acid, 75 mL propionic acid and 35 mL nitrobenzene were refluxed at 150 °C (1.5 h). Then reaction mixture temperature was lowered to about 50-60 °C and air was blown (30 min) and then 35 mL petroleum ether was added and this mixture was nightly kept in the refrigerator. Then the precipitate was collected and washed with petroleum ether. Then, the precipitate was washed in the Soxhlet extractor with ethyl acetate, synthesized porphyrin was dissolved in ethyl acetate but by-products were not dissolved in ethyl acetate. The porphyrin was characterized by ^{13}C NMR, ^{1}H NMR, UV-Vis and FT-IR.

THPP: ^{13}C NMR ($CDCl_3$ δ, 400 MHz): 114.383 (meso-C), 120.738 (β-C), 132.237-136.070 (Aromatic carbons), 157.790 (α-C). ^{1}H NMR (500 MHz, DMSO, ppm, TMS reference): 7.989-8.010 (H-orto, m, 8H), 7.198-7.219 (H-meta, m, 8H), 8.866 (H-pyrrole, s, 8H), 9.983 (OH, s, 4H), -2.887 (NH, br s, 2H). FT-IR (film on KBr, cm^{-1}): 1466 (C-N), 1605 (C Aromatic), 2366 (N-H), 2923 (C-H), 3426 (O-H). Visible (dichloromethane) λ nm (ε (M^{-1} cm^{-1})): 418 (3.3×10^5), 642 (3.2×10^2), 585 (1.5×10^2), 543 (1.1×10^2) and 513 (1.1×10^2).

The MTHPP complex was obtained from the reflex of THPP and $MCl_3 \cdot 4H_2O$ or $MCl_2.6H_2O$ (M = Co^{III}, Zn^{II}, Ni^{II}) in ethyl acetate (8 h) according to the Alder *et al.* method [35] that chemical structure of MTHPP (M = Co^{III}, Zn^{II}, Ni^{II}) was shown in Scheme 1. The metalloporphyrins were studied by techniques of UV-Vis and FT-IR.

Analytical calculation for MTHPP, FT-IR (KBr, cm^{-1}): 1421 (C-N), 1600 (C=C, Aromatic), 2930 (C-H), 3430 (O-H). Visible light (chloroform): λ nm (ε (M^{-1} cm^{-1})): 415 (3.13×10^5, 530 (1.6×10^2).

The Preparation of the (Fe_3O_4@SiO_2@TiO_2@ MTHPP) (MSiTMP) (M = Co^{III}, Zn^{II}, Ni^{II}) Nanocomposites

0.04 g MTHPP (M = Co^{III}, Zn^{II}, Ni^{II}) (metaltetra-hydroxylphenylporphyrin) was dissolved in 20 mL of absolute ethanol (Solution 1). 0.08 g MSiT was dipped in 20 mL of absolute alcohol. Solution 1 was placed under ultrasonic treatment (30 min), resulted dark red solution was transferred to the flask that contained MSiT. This mixture stirred at r.t (one day), then the solvent was evaporated by rotary evaporator. MSiTMP (M = Co^{III}, Zn^{II}, Ni^{II}) nanocomposites were recovered, washed with distilled water in order to remove impurities and unreacted reactants. The magnetic nanocomposites were separated by a strong magnet. Finally, the magnetic products were dried in vacuum desiccator at r.t for one day.

Characterizations

The morphologies of the nanocomposites were observed by the LEO-1455VP microscope (acceleration voltage 10 kV) scanning electron microscopy (SEM) analyses equipped with energy dispersive X-ray spectrometry (EDS) and transmission electron microscope (TEM, Zeiss-EM10C-100 KV). Infrared spectra were recorded in KBr pellet by a FT-IR Bruker instrument. ^{13}C NMR, ^{1}H NMR spectra were recorded on a Bruker Avance III-400 MHz spectrometer and tetramethylsilane (TMS) as reference. The UV-Vis-Diffuse reflectance spectroscopy (DRS) study of nanocomposites was done on a Shimadzu (MPC-2200) spectrophotometer. The X-ray powder patterns (XRD) were performed with a Bruker D8 diffractometer (Cu Kα irradiation) in the 2θ range 20-80°. The vibrating sample magnetometer (VSM, Maghnatis Kavir Kashan Co, Iran) was employed to study the magnetic properties of Fe_3O_4 nanoparticle, MSi, MSiT and MSiTMP nanocomposites at room temperature from 1000 to + 10000 Oe. INC-Belsorp II apparatus was used for measurement of the nitrogen adsorption at 77 K. A JASCO Spectrofluorometer (Model FP-8300) was used for measurement of Photoluminescence (PL) using a xenon lamp at r.t and the used excitation wavelength (λ_{ex}) was 325 nm.

Photocatalyst Test

Photocatalytic activity studies of the MSiTMP (M = Co^{III}, Zn^{II}, Ni^{II}) nanocomposites were investigated by the degradation of MB solution. The reactions were carried out in a cylindrical photoreactor, which contained 100 mL MB solution and 0.01 g of photocatalyst (MSiTMP (M = Co^{III}, Zn^{II}, Ni^{II}) and MSiT nanocomposites). The mixture was kept in dark for 2 h to allow the mixture to reach adsorption-desorption equilibration. The irradiations were undertaken utilizing a four blue Vis-LED lamps mounted photolysis box (4 × 3 W power, λ = 465 nm) with no cut-off filter. A tube containing the mixture was place at the center of box and at a 10 cm distance from the lamps. The photodegradation was performed at room temperature and since heat production of LED lamps is low no cooling device was needed. The oxygen was continually blown at the MB solution. The photodegradation of MB was investigated by measuring the concentrations of the MB solution by a UV-Vis Spectrophotometer (Baric 2100 model) at 662 nm wavelengths during the reaction. For studying of reusability of photocatalysts, after the end of the photodegradation reaction, photocatalysts separated with a strong magnet, and eluted several times with water and dried in vacuum desiccator at r.t for one day.

RESULTS AND DISCUSSION

Characteristics of the Photocatalysts

The interaction between metalloporphyrin and MSiT is confirmed with the FT-IR spectra of Co^{III}THPP, Zn^{II}THPP, Ni^{II}THPP and MSiTMP (M = Co^{III}, Zn^{II}, Ni^{II}) nanocomposites. As indicated in Fig. 1, the peak at about ~ 3426 cm^{-1} can be attributed to the stretching vibration of hydroxyl groups that play the main role in the connection of MTHPP (M = Co^{III}, Zn^{II}, Ni^{II}) on the surface of MSiT nanocomposite. The observed bands at 3436 cm^{-1} and 1605 cm^{-1} are related to the OH vibrations of the water. The two stretching modes are observed at 570 and 462 cm^{-1} that are assigned to the Fe-O-Fe bonds in M nanoparticles. The broad bands at 962, and 1095 cm^{-1} are related to the asymmetric stretching vibration of and Si-OH, and Si-O-Si

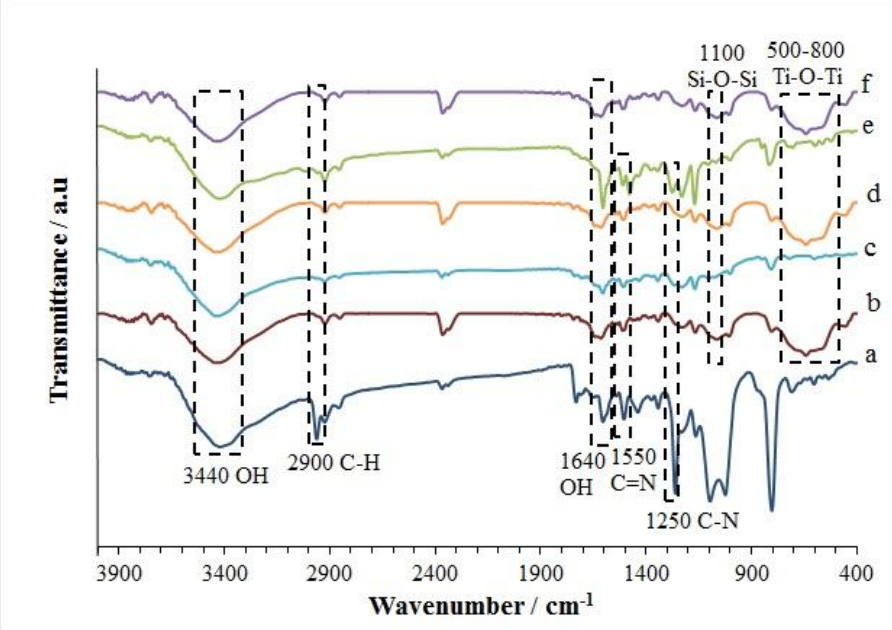

Fig. 1. The FT-IR spectra of (a) Ni^{II}THPP (b) MSiTNi^{II}P (c) Zn^{II}THPP (d) MSiTZn^{II}P (e) Co^{III}THPP and (f) MSiTCo^{III}P.

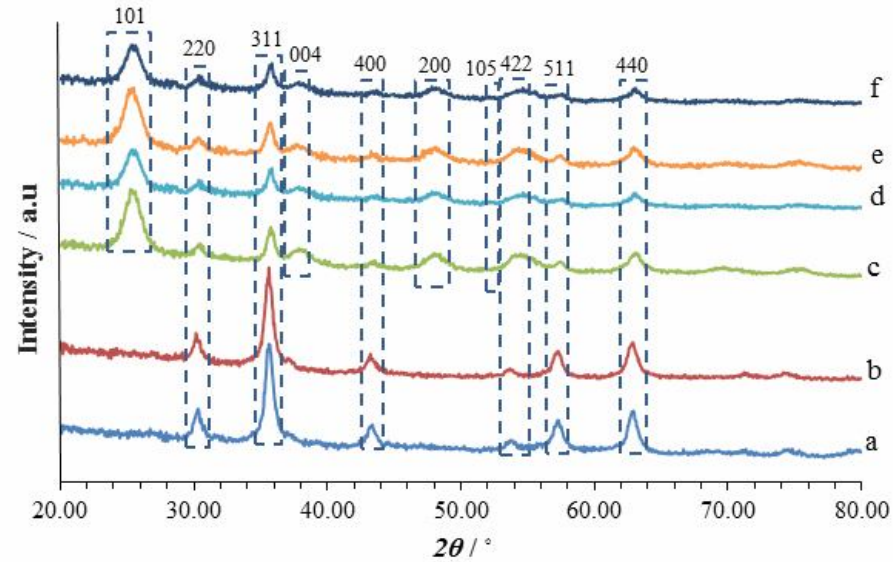

Fig. 2. The XRD pattern of (a) M (b) MSi (c) MSiT (d) MSiTCo^{III}P (e) MSiTNi^{II}P and (f) MSiTZn^{II}P.

bonds. These results indicated that the M surface is covered with the silica layer. The FT-IR spectrum of MSiTMP (M = Co^{III}, Zn^{II}, Ni^{II}) nanocomposites exhibit vibration bands in the ranges of 500-800 cm^{-1} that is due to stretching vibration of Ti-O-Ti bonds in TiO_2. The MSiTMP (M = Co^{III}, Zn^{II}, Ni^{II}) nanocomposites have vibration bands at around 722, 1250, 1550, 1605, 1640 and 2900 cm^{-1} which can be attributed to metal-ligand, C-N, C=N, C=C, O-H and C-H

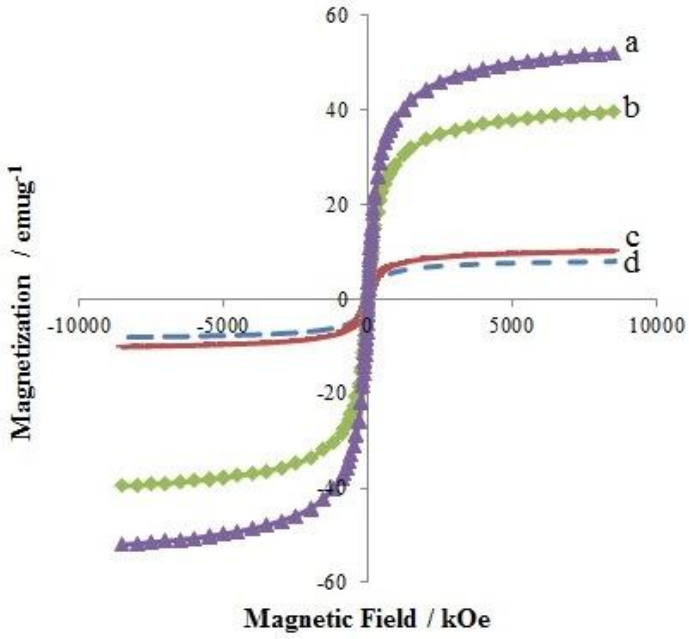

Fig. 3. The VSM curves of (a) M (b) MSi (c) MSiT and (d) MSiTMP (M = Co^{III}, Zn^{II}, Ni^{II}).

bonds respectively. These results indicated that the porphyrins were successfully attached on the MSiT nanocomposite.

The XRD patterns of M, MSi, MSiT, MSiTMP (M = Co^{III}, Zn^{II}, Ni^{II}) nanocomposites are illustrated in Fig. 2. The Fig. 2a shows XRD pattern of M with six diffraction peaks at 30° (220), 36° (311), 43° (400), 54° (422), 57° (511) and 63° (440) which are consistent with the highly pure cubic phase of Fe_3O_4 (JCPDS file No. 19-0629). From these XRD data (Fig. 2a) the average crystalline size (L) of Fe_3O_4 nanoparticles was calculated to be 13 nm by Debye-Scherrer Eq. (1) [36,37],

$$L = \frac{K\lambda}{\beta \cos\theta} \quad (1)$$

where λ is the wavelength of X-ray (nm); L is crystallite size (nm); K is a dimensionless shape factor, which usually has a value of about 0.9; β is the width of the diffraction peak at its half intensity maximum in radians (θ). No distinct peak was observed for SiO_2 which implying that the synthesized SiO_2 is amorphous [38] (Fig. 2b). The XRD pattern of MSiT (Fig. 2c) shows all above-mentioned diffraction peaks of M as well as four new diffraction peaks at 52° (105), 48° (200), 38° (004) and 25° (101) which is the well-known diffraction pattern of anatase TiO_2 (with standard card JCPDS No. 21-1272). The peaks intensity of MSiT nanocomposite was decreased in comparison with Fe_3O_4 which is due to the coating of SiO_2 and TiO_2 layers. The XRD results demonstrated that the crystalline anatase TiO_2 and Fe_3O_4 coexist in MSiT nanocomposites. The average crystallite size of MSiT nanocomposite calculated by XRD data by Debye-Scherrer equation is 8 nm. Figure 2d, e and f illustrated the XRD patterns of MSiTCo^{III}P, MSiTNi^{II}P, and MSiTZn^{II}P, respectively. The patterns show that the initial characteristic peaks of the MSiT nanocomposite remained unchanged. The results shown in Figs. 2d, e and f revealed that loading the porphyrins on the TiO_2 has little effect on the crystal chemistry of MSiT nanocomposite. The XRD peak position and width of MSiTMP (M = Co^{III}, Zn^{II}, Ni^{II}) nanocomposites are the same as those of MSiT nanocomposite.

The VSM curves of the M, MSi, MSiT and MSiTMP (M = Co^{III}, Zn^{II}, Ni^{II}) are shown in Fig. 3. The magnetic saturation values for M, MSi, MSiT and MSiTMP (M = Co^{III}, Zn^{II}, Ni^{II}) particles are 52, 39.6, 10.10 and

Table 1. The BET Surface Areas and Average Pore Widths of Synthesized Nanoparticles

Sample BET	Surface area ($m^2 g^{-1}$)	Average pore widths (nm)	Vg_{BJH} ($cm^3 g^{-1}$)
M	30.7	5.23	0.03
MSi	71.0	6.04	0.10
MSiT	129	6.56	0.20

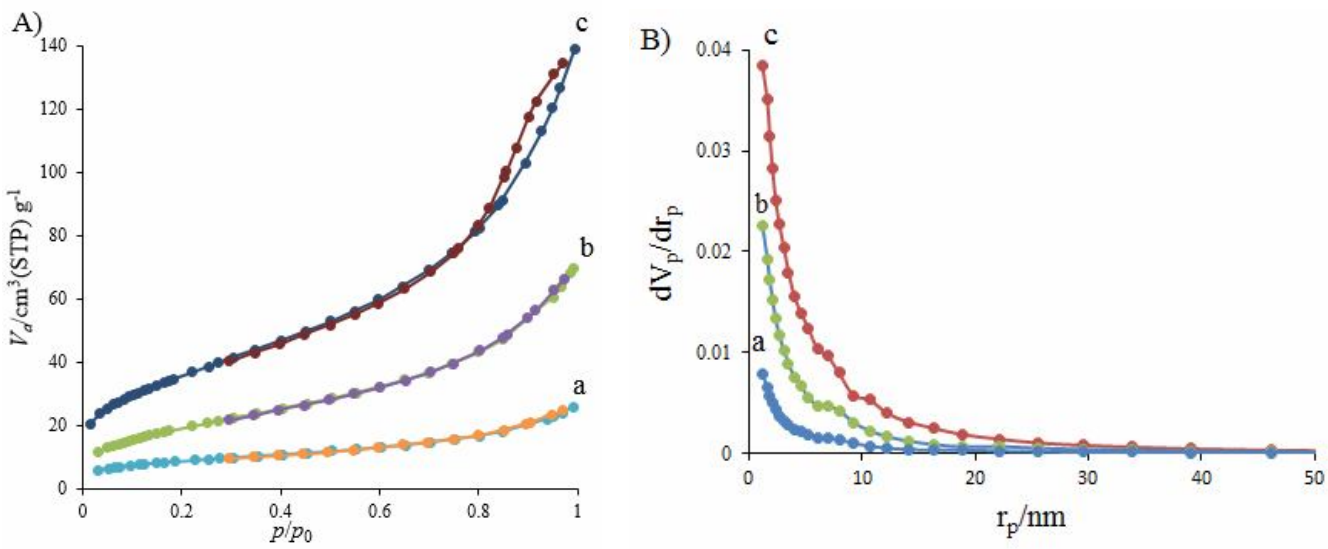

Fig. 4. (A) The N_2 adsorption-desorption isotherm for (B) BJH diagrams of (a) M (b) MSi (c) MSiT.

8.03 emu g^{-1}, respectively (Figs. 3a-d). Small values of remanent magnetization (Mr) and coercivity (Hc), the absence of hysteresis phenomenon, and no obvious remanence effect show that the magnetic nanocomposites have superparamagnetic behavior at room temperature. The saturation magnetization of M (52 emu g^{-1}) gradually decreases upon coating with silica, titania, and MTHPP (M = Co^{III}, Zn^{II}, Ni^{II}), The hysteresis loops of the MSi, MSiT and MSiTMP (M = Co^{III}, Zn^{II}, Ni^{II}) nanocomposites are lower than that of Fe_3O_4; it means that the nonmagnetic covered layers, namely silica, titania and MTHPP (M = Co^{III}, Zn^{II}, Ni^{II}), reduce the magnetization of the samples. However, the magnetism of MSiTMP (Fig. 3d) was still high to be separated by a strong magnet.

The N_2 adsorption-desorption data are summarized in Table 1 and illustrated in Fig. 4, including BJH (Barrett, Joyner and Halenda) pore volume, Brunauer-Emmett-Teller (BET) surface area, and average pore widths for M, MSi and MSiT, respectively. There is a significant increase in pore volume and surface area of prepared nanoparticles with respect to magnetite (M). The porous materials tend to adsorb MB on the surface and promote the photocatalytic process and increase the rate of the photodegradation process. The further pore volume and surface area of the photocatalyst can generally increase the photodegradation rate.

Figure 5 shows SEM images of M, MSi, MSiT and MSiTMP (M = Co^{III}, Zn^{II}, Ni^{II}) nanocomposites. As

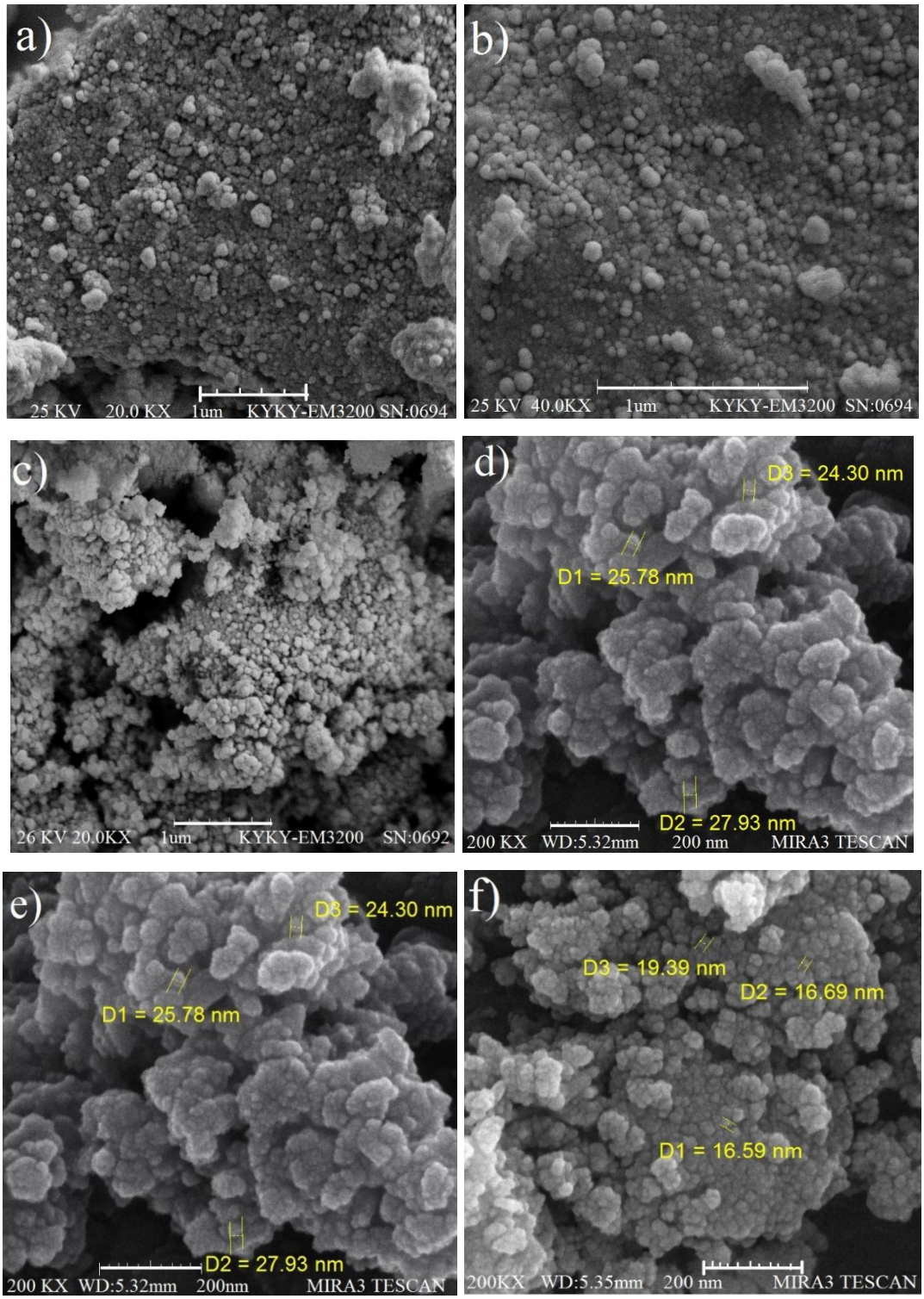

Fig. 5. The SEM images of (a-c) M, MSi, and MSiT images and (d-f) images of MSiTNi^{II}P, MSiTCo^{III}P and MSiTZn^{II}P nanocomposites.

observed in Figs. 5a-c, the most of the M nanoparticles, MSi and MSiT nanocomposites are fine with almost spherical morphology in the range of 18-40nm. As indicated in Figs. 5d-f, the most of MSiTMP (M = Co^{III}, Zn^{II}, Ni^{II}) nanocomposites have approximately spherical morphology in the range of 17-30 nm. The TEM images of MSiT, MSiTNi^{II}P, MSiTCo^{III}P and MSiTZn^{II}P nanocomposites (Fig. 6) further confirm the results and revealed the core-shell structure of MSiTMP nanocomposites. The results were clearly supported the loading of THPP on the surface of the MSiT nanocomposite.

The EDS results of MSiTMP (M = Co^{III}, Zn^{II}, Ni^{II}) nanocomposites are presented in Table 2, and confirm the presence of C, O, N, Fe, Ti, Ni, Zn, Co and Si in MSiTMP (M = Co^{III}, Zn^{II}, Ni^{II}) nanocomposites. The results clearly indicate the loading of MTHPP (M = Co^{III}, Zn^{II}, Ni^{II}) on the MSiT nanocomposite.

UV-Vis-DRS spectra of the MSiT and MSiTMP (M = Co^{III}, Zn^{II}, Ni^{II}) nanocomposites are shown in Fig. 7A (a-d). As, it can be observed in Fig. 7A, the spectra of MSiTMP (M = Co^{III}, Zn^{II}, Ni^{II}) nanocomposites are red shifted compared to the MSiT nanocomposite which implying that the sensitizing abilities of the MTHPP (M = Co^{III}, Zn^{II}, Ni^{II}) in MSiT nanocomposite happening through displacement of the sensitizer optical absorption edge from ultra-violet to the visible region. The band gap energy (E_g) is calculated from a plot of $(F(R_\infty)h\nu)^{1/2}$ *vs*. hν as shown in Fig. 7B. From the spectra, the band gap for nanocomposites are calculated according to the Kubelka-Munk function ($(F(R_\infty)$, Eq. (2)).

$$F(R_\infty) = \frac{K}{S} = \frac{(1-R_\infty)^2}{2R_\infty} \quad (2)$$

Where $R_\infty = \frac{R_{sample}}{R_{standard}}$ is the reflectance of an infinitely thick specimen, while K and S are the absorption and scattering coefficients, respectively [39]. Putting $F(R_\infty)$ instead of α into Tauc equation (Eq. (3)) results in the Eq. (4).

$$(\alpha . h\vartheta)^{1/2} = B(h\vartheta - E_g) \quad (3)$$

$$(F(R_\infty) . h\vartheta)^{1/2} = B(h\vartheta - E_g) \quad (4)$$

The band gap for MSiT, MSiTCo^{III}P, MSiTZn^{II}P and MSiTNi^{II}P nanocomposites are estimated to be 2.6, 2.5, 2.4 and 2.2 eV, respectively (Fig. 7B). The results revealed that due to the doping of TiO_2 with Fe_3O_4, the band gap of MSiT nanocomposite is lower than that of pure TiO_2 (3.2 eV). A further decrease of band gap occurs in MSiTMP (M = Co^{III}, Zn^{II}, Ni^{II}) nanocomposites which can be related to the sensitizing effect of the MTHPP (M = Co^{III}, Zn^{II}, Ni^{II}). Photoluminescence spectra (PL) was used to investigate the life of electron-hole pairs in semiconductors [40,41].

Figure 8 shows the photoluminescence spectrum of pure MSiT nanocomposite (spectrum a) and MSiTMP (M = Co^{III}, Zn^{II}, Ni^{II}) nanocomposites (spectra b-c) with λ_{ex} = 325 nm. The spectra of these nanocomposites show similar emission peak pattern. However, the emission spectrum of TiO_2 is quenched upon sensitization with the MTHPP (M = Co^{III}, Zn^{II}, Ni^{II}). Also, the quenching behavior indicated that the excited electrons in the MSiTMP (M = Co^{III}, Zn^{II}, Ni^{II}) nanocomposites could be more effectively transferred than that in MSiT nanocomposite. It is due to fact that charge transfer between MTHPP (M = Co^{III}, Zn^{II}, Ni^{II}) and MSiT nanocomposite results in more separation efficiency of the generated electrons in the MSiTMP (M = Co^{III}, Zn^{II}, Ni^{II}) nanocomposites than that in MSiT. With respect to the results given in Fig. 8, feasibility of electron transfer follows the order: MSiTNi^{II}P > MSiTZn^{II}P > MSiTCo^{III}P > MSiT.

Photodegradation Studies

The photodegradation of MB solution was studied in the presence of the MSiTMP (M = Co^{III}, Zn^{II}, Ni^{II}) photocatalysts under the blue Vis-LED lamps irradiation. The effect of several factors, such as the type of photocatalyst, oxygen and light on the degradation of MB was investigated. Figures 9A-D indicates the time dependent UV-Vis spectra photodegradation of MB in the presence of MSiTMP (M = Co^{III}, Zn^{II}, Ni^{II}) and MSiT photocatalysts, respectively. The dark condition (spectrum b) was tested to investigate the absorption of MB on the surface of photocatalysts. The results indicate that adsorption of MB on MSiTMP (M = Co^{III}, Zn^{II}, Ni^{II}) nanocomposites is more than that on MSiT nanocomposite. Higher adsorption of MB on the photocatalysts results in higher photodegradation efficiency. Figure 10 shows that irradiation time of light, O_2 and nature of sensitizers are

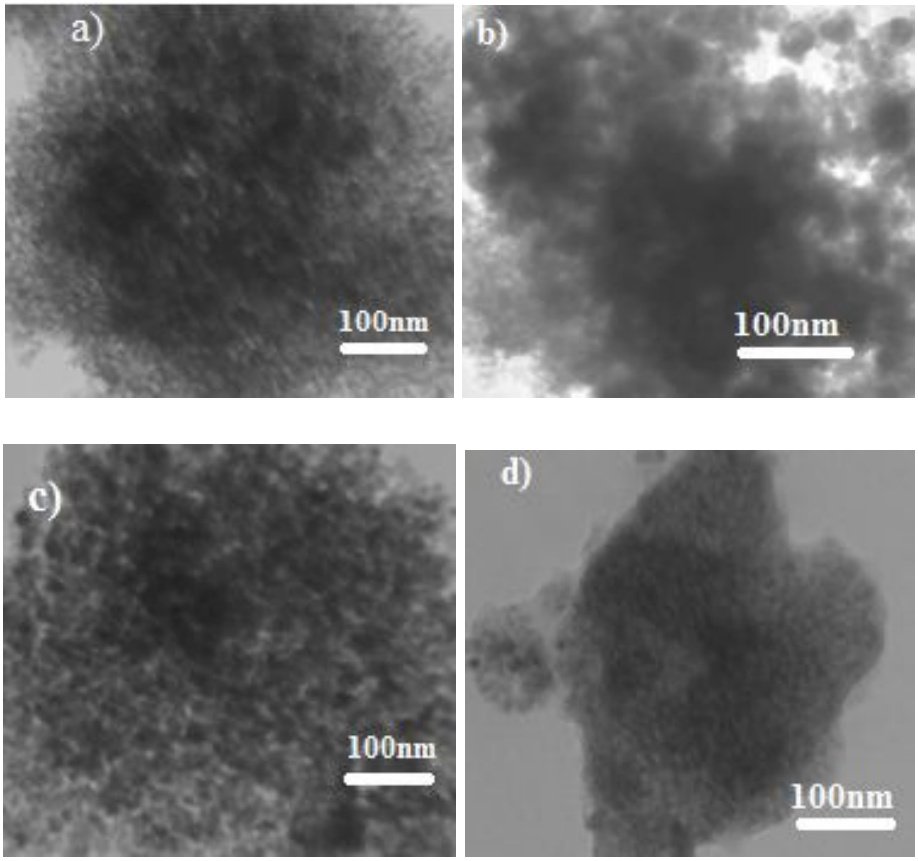

Fig. 6. The TEM images of (a) MSiT (b) MSiTNi^{II}P (c) MSiTCo^{III}P and (d) MSiTZn^{II}P nanocomposites.

Table 2. Quantitative Results of EDS Spectrum

Elements	Weight percent of nanocomposite		
	MSiTCo^{III}P	MSiTNi^{II}P	MSiTZn^{II}P
C	18.2	25.6	19.0
N	4.50	11.4	3.40
O	29.0	38.0	27.0
Si	3.00	2.70	2.50
Ti	30.8	12.3	28.4
Fe	13.9	10.0	18.5
Metal (Co^{III}, Ni^{II}, Zn^{II})	0.60	0.20	1.40
Total	100	100	100

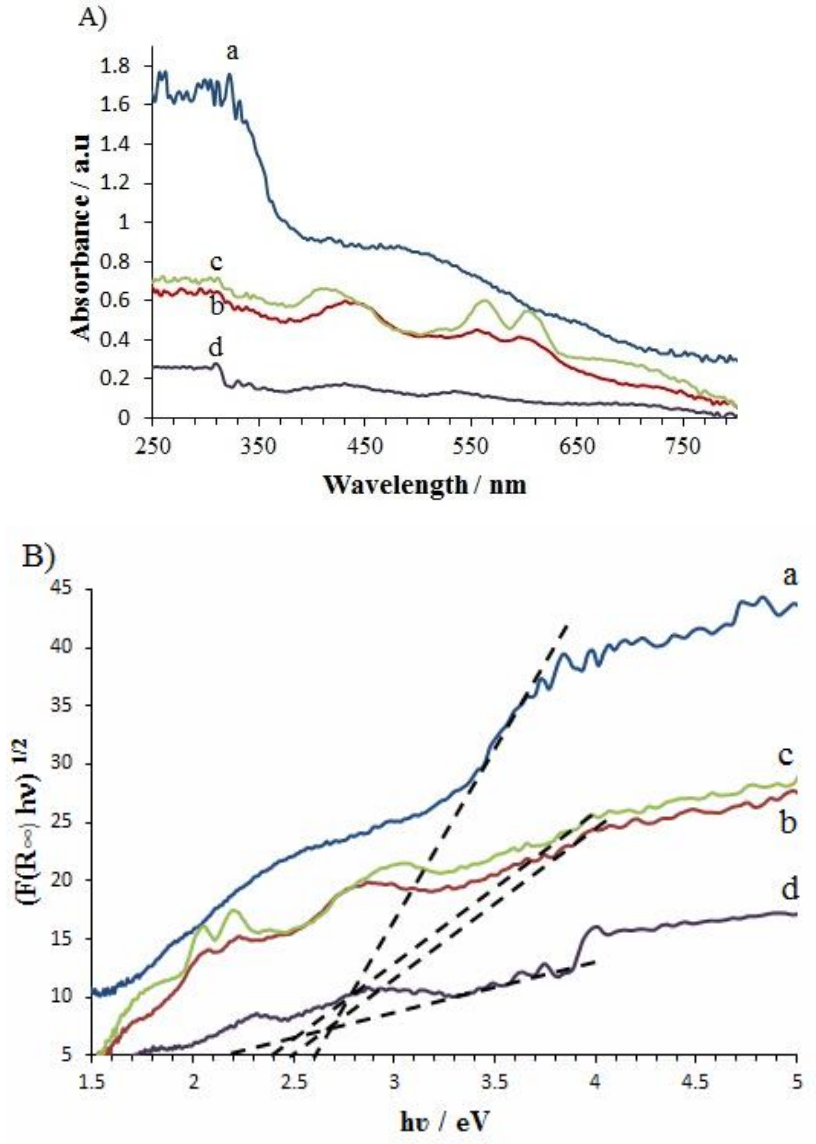

Fig. 7. A) The UV-DRS of (a) MSiT **(**b) MSiTCo^{III}P (c) MSiTZn^{II}P and d) MSiTNi^{II}P. B) Plot of $(F(R\infty)h\nu)^{1/2}$ *vs*. photo energy (hν) of (a) MSiT **(**b) MSiTCo^{III}P (c) MSiTZn^{II}P and (d) MSiTNi^{II}P nanocomposites.

most important factors affecting the rate and efficiency of photocatalyic degradation of MB. As expected, all the three photocatalysts MSiTMP (M = Co^{III}, Zn^{II}, Ni^{II}) exhibit enhanced photocatalytic activitites with respect to MSiT nanocomposite based on the following order: MSiTNi^{II}P > MSiTZn^{II}P > MSiTCo^{III}P > MSiT. Figure 10 is obtained based on the degradation rate (D) which can be calculated using Eq. (5).

$$D = \frac{A_0 - A_i}{A_0} \quad (5)$$

In Eq. (5), A_0 is absorption of MB in the absence of photocatalyst before irradiation at 662 nm wavelength, A_i is absorption of the MB after irradiation time t. The result exhibited that the photocatalytic activity of MSiTNi^{II}P is more than that of MSiTZn^{II}P and MSiTCo^{III}P photocatalysts (as displayed in Figs. 10a-c), which may be related to the

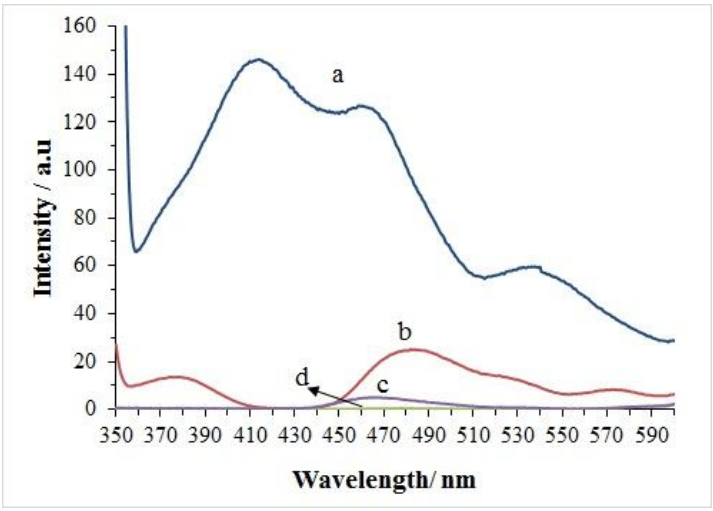

Fig. 8. The photoluminescence spectra of samples (a) MSiT (b) MSiTCo^{III}P (c) MSiTZn^{II}P and (d) MSiTNi^{II}P nanocomposites at room temperature.

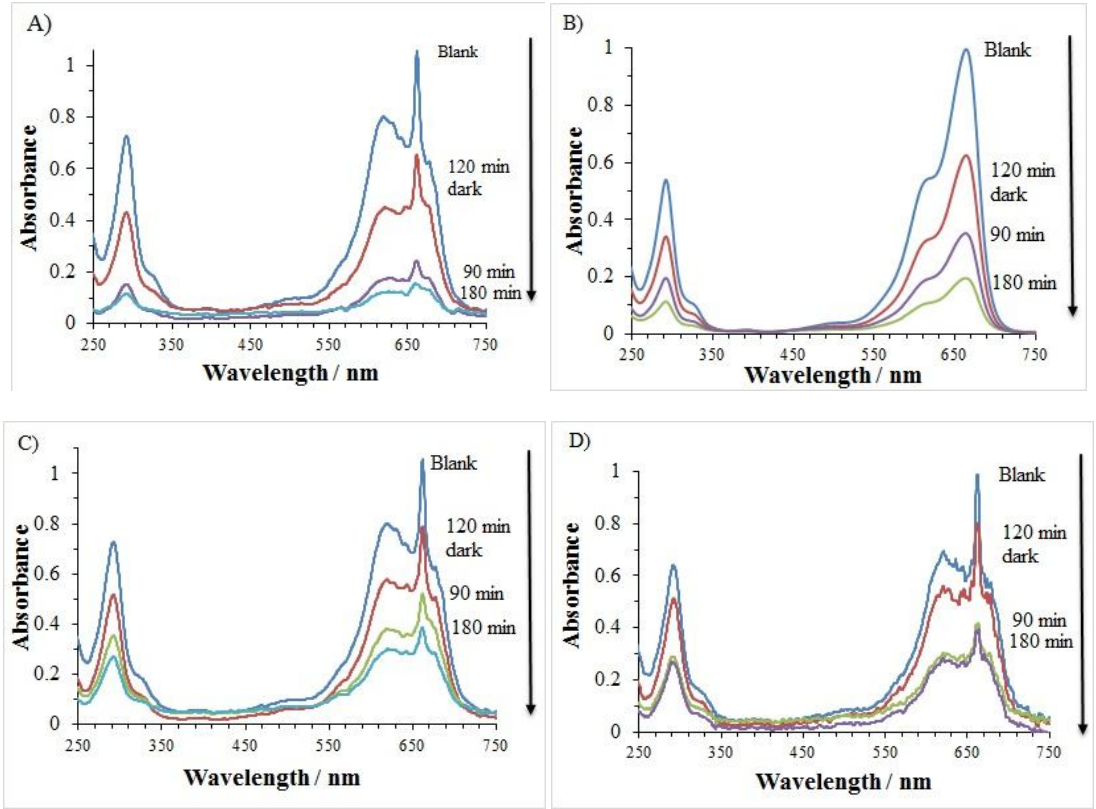

Fig. 9. The absorbance changes *vs*. wavelength (nm) for MB on the surface of (A) MSiTNi^{II}P (B) MSiTZn^{II}P (C) MSiTCo^{III}P and (D) MSiT (initial concentration: 7 mg L^{-1}, 100 mL, and 0.01 g of photocatalyst, under blue LED light irradiation).

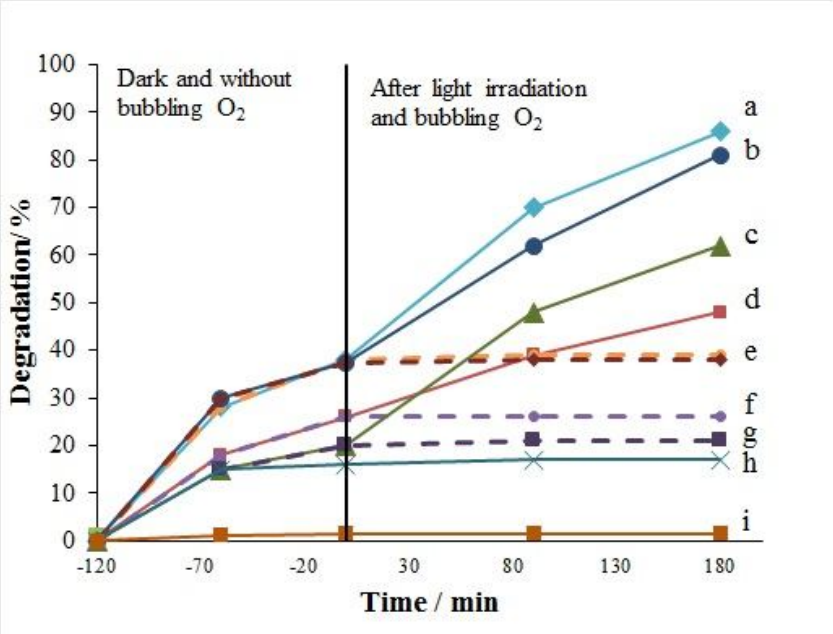

Fig. 10. Degradation percent of the MB solution using (a) MSiTNi^{II}P (b) MSiTZn^{II}P (c) MSiTCo^{III}P (d) MSiT photocatalysts in the presence of O_2 and light, (e) MSiTZn^{II}P, MSiTNi^{II}P (f) MSiT (g) MSiTCo^{III}P photocatalyst in absence O_2 and light (h) Only in the presence of O_2 and (i) Only in the presence of light.

fact that the excited potential of MSiTNi^{II}P photocatalyst is best match with CB of TiO_2 potential, and implying key role of central metal in photosensitizing ability of the porphyrins [20]. The results of present study, together with data obtained in previous studies for photocatalytic degradation of some pollutants are summarized in Table 3 [6,23,27,42-48]. The comparison revealed that the photocatalysts used in present research have several advantages including milder reaction conditions, shorter reaction time, removal of homogeneous photocatalysts, high yield of the reaction, easy recovery of photocatalyst, and the reusability of the photocatalyst.

Kinetics Study

The kinetic of photodegradation treatments of MB were investigated and their results are shown in Figs. 11a-e. It is observed that these processes follow pseudo first order kinetics. Therefore, the Langmuir-Hinshelwood model can be utilized to explain these processes [20]. These kinetics can be represented with the Eq. (6):

$$\ln\left(\frac{C_0}{C_i}\right) = K_{appt} \tag{6}$$

Where t, C_i, C_0, K_{app} (min^{-1}) are the irradiation time (min), the concentration of MB at irradiation time t, the initial concentration of MB before irradiation, and the apparent rate constant, respectively. The rate constants are used for comparison of the photocatalytic activities between MSiT and MSiTMP (M = Co^{III}, Zn^{II}, Ni^{II}) nanocomposites, as are presented in Fig. 11.

Removal Mechanism Study

The pure TiO_2 has a band gap energy which is 3.2 eV, lead to the result that TiO_2 photocatalyst can be activated only in the UV light range [49]. The band gap of MSiT nanocomposite (2.6 eV) is lower than pure TiO_2 due to the presence of Fe_3O_4 [50]. The band gap value of MSiT nanocomposite can be further decreased in presence of

Table 3. Comparison of the Results of Present Study with Previously Reported Data for Photodegradation of some Organic Compounds

Entry	Pollutant type	Catalytic system	Reaction conditions	Yield	Ref.
1	4-Nitrophenol	Cu^{II}, Co^{II}, Zn^{II}-Carboxyl porphyrins-TiO_2	400W halogen lamp, air, cooling with circular water running, 60 min, catalyst dose = 200 mg L^{-1}	100%	[1]
2	Phenol and carbamazepine	$Fe_3O_4/SiO_2/TiO_2$ $CoFe_2O_4/SiO_2/TiO_2$ $BaFe_{12}O_{19}/SiO_2/TiO_2$	300W Xenon Lamp (UV-Vis light), 120 min, catalyst dose = 2000 mg L^{-1}	95% 85% 20%	[6]
3	4-Nitrophenol	Mn^{II}, Fe^{II}, Cu^{II}-5, 10, 15, 20-tetra-(4-tert-butyl phenyl) porphyrin-TiO_2	125W medium pressure Hg lamp (UV-lamp), O_2, cooling with circular water running, 3 h, catalyst dose = 800 mg L^{-1}	100%	[16]
4	Methyl orange	TiO_2/Zn or Sn (5-(p-hydroxyl phenyl)-10,15,20-triphenyl porphyrin	1000W iodine-tungsten lamp, in air, 180 min, catalyst dose = 10 mg L^{-1}	50% 85%	[21]
5	4-Nitrophenol	Cu^{II}, Zn^{II}, Ni^{II}-5-mono-[4-(2-(4-hydroxy)-phenoxy)ethoxy]-10,15, 20-triphenyl porphyrin-TiO_2	400W halogen lamp, air, cooling with circular water running, 66 min, pH= 6.40, catalyst dose = 200 mg L^{-1}	75%	[22]
6	MB	$Fe_3O_4/SiO_2/mTiO_2$	250W high pressure Hg lamp (365 nm), 90 min, catalyst dose = 500 mg L^{-1}	90%	[39]
7	MB	$SrFe_{12}O_{19}/SiO_2/TiO_2$	UV-lamp (20W), 180 min, catalyst dose = 600 mg L^{-1}	80%	[40]
8	Rhodamine B (RhB)	Fe_3O_4/TiO_2/Ag, Cu	500W high pressure mercury lamp, 90 min, catalyst dose = 1000 mg L^{-1}	86%	[41]
9	Dimethyl phthalate	$Fe_3O_4/SiO_2/TiO_2$/copper phthalocyanine	55W Xenon lamp, O_2, 12 h, catalyst dose = 1200 mg L^{-1}	45%	[42]
10	4-Nitrophenol	TiO_2/Cu-5-(4-hydroxy)phenyl)-10,15, 20 triphenyl porphyrin	350W Xenon lamp (380-780 nm), 300min, catalyst dose = 100 mg L^{-1}	95%	[43]
11	MB	$Fe_3O_4/SiO_2/TiO_2/Co^{III}$, Zn^{II}, Ni^{II} tetrahydroxylphenylporphyrin	3W Blue-LED lamp, 180 min, bubbling O_2, catalyst dose = 100 mg L^{-1}	90%, 80%, 63%	This work

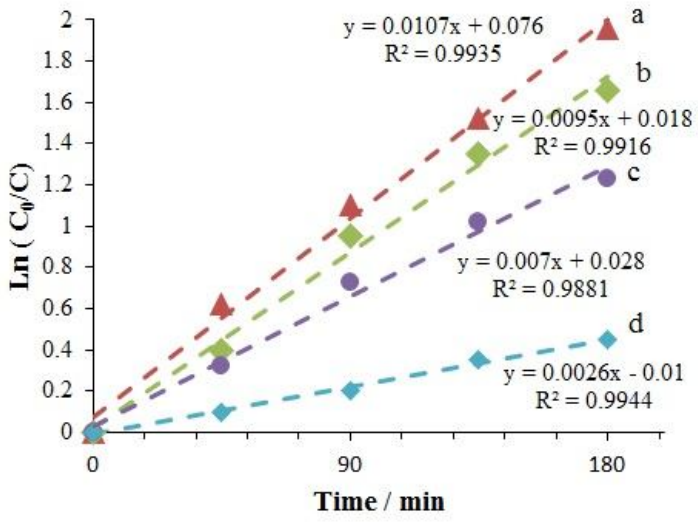

Fig. 11. The kinetics of MB photocatalytic degradation using (a) MSiTNi^{II}P (b) MSiTZn^{II}P (c) MSiTCo^{III}P and (d) MSiT photocatalysts.

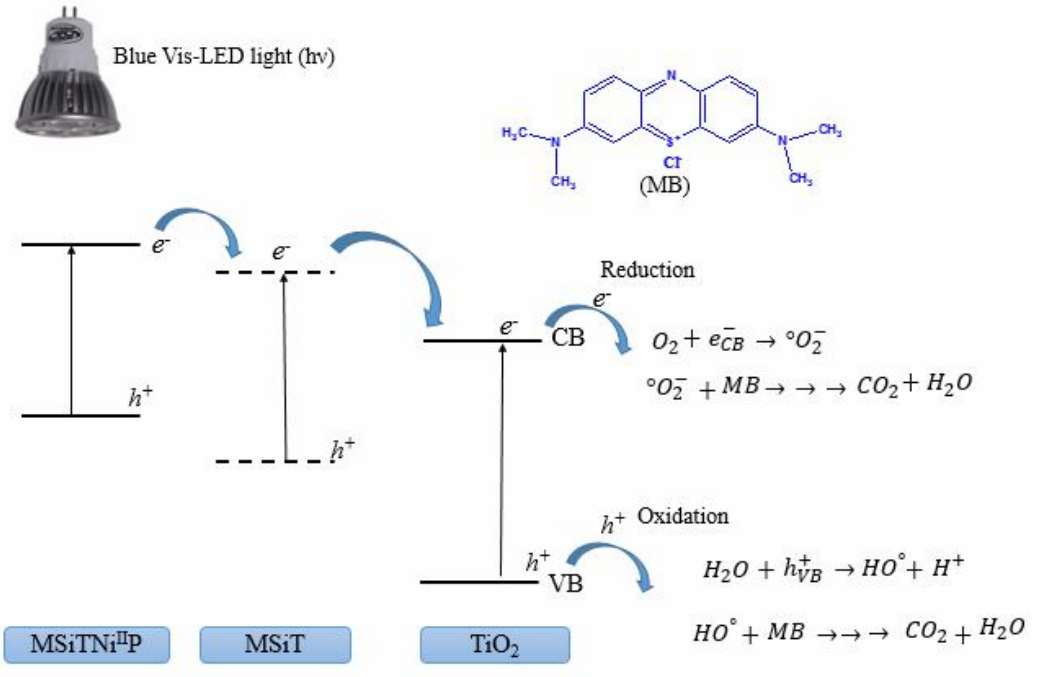

Scheme 2. The possible mechanism of the photodagradation of MB by MSiTNi^{II}P nanocomposite

porphyrin photosensitizer [51]. A possible mechanism for the photdegradation of MB has been presented in Scheme 2. It is assumed that when MSiTMP nanocomposites are irradiated with visible light, electrons are excited from the valence band (VB) of the MTHPP to its conduction band (CB) and construct holes in the VB. The excited singlet

MTHPP[1] can pass by intersystem crossing (ISC) mechanism into the triplet MTHPP[3] (the Eq. (7)) [47]. Then the long live MTHPP[3] can transfer electron into (CB) of the TiO_2 support and finally these electrons are transferred to the most stable molecular oxygen ($^3O_2$) to create active oxygen species ($^{\bullet}O_2^-$) and ($^1O_2$), which MB can be degraded by active oxygen (the Eq. (8) and (9)). The water can oxidize to $^{\bullet}OH$ in aqueous medium holes in VB of TiO_2 and generated radicals can degrade MB to small organic molecules or CO_2, H_2O. The results show that MSiTMP (M = Co^{III}, Zn^{II}, Ni^{II}) nanocomposites have a higher photodegradation efficiency compared with the MSiT. Mainly, three active agents, namely superoxide anion radical ($^{\bullet}O_2^-$), hydroxyl radical ($^{\bullet}OH$), and holes (h^+) interfere with the photocatalytic activity reaction in the degradation of MB. The photocatalytic mechanism using these agent gives as follow (the Eqs. (7)-(13)):

$$MTHPP + h\upsilon \rightarrow MTHPP^{1+} \rightarrow MTHPP^{3+} \quad (e_{CB}^-) + h_{VB}^+) \, (ISC) \tag{7}$$

$$MTHPP^{3+} + {}^3O_2 \rightarrow MTHPP + {}^1O_2 \tag{8}$$

$$MTHPP^{3+} + {}^3O_2 \rightarrow MTHPP^+ + {}^{\circ}O_2^- \tag{9}$$

$$H_2O + h_{VB}^+ \rightarrow HO^{\circ} + H^+ \tag{10}$$

$${}^1O_2 + MB \rightarrow CO_2 + H_2O \tag{11}$$

$${}^1O_2 + MB \rightarrow CO_2 + H_2O \tag{12}$$

$$HO^{\circ} + MB \rightarrow CO_2 + H_2O \tag{13}$$

Reusability of Photocatalysts

In view of significant ferromagnetic characteristic of the investigated photocatalysts, they can be separated from the reaction solution by a strong magnet. Moreover the reusability of the heterogonous photocatalysts can be regard as an advantageous characteristic and may be of significant interest. The stability and reusability of the photocatalysts were studied for several times. The recycled photocatalysts were used in the new photodegradation reaction of MB at the same conditions. The degradation percent of MB on surface of MSiTNi^{II}P, MSiTZn^{II}P, MSiTCo^{III}P and MSiT photocatalysts in three consecutive cycles were 90, 82 and 75% g^{-1}; 80, 75 and 62% g^{-1}; 63, 56 and 50% g^{-1}; 48, 42 and 35% g^{-1}, respectively, which showed that the photocatalytic activity of the photocatalysts was nearly constant.

CONCLUSIONS

The Co^{III}, Zn^{II}, Ni^{II} complexes of tetrahydroxylphenyl-porphyrin, MSiTMP (M = Co^{III}, Zn^{II}, Ni^{II}) nanocomposites, were prepared and appended on silica coated magnetic TiO_2 and employed in the photocatalytic degradation of MB solution under the blue LED irradiation. The presence of four hydroxyl group on the porphyrin moiety led to their tight binding on the surface of TiO_2, which was evidenced by several analytical methods including XRD, VSM, DRS-UV-Vis, SEM, EDS and FT-IR spectroscopy. All of the three photocatalysts MSiTMP (M = Co^{III}, Zn^{II}, Ni^{II}) showed more photocatalytic activity with respect to the MSiT nanocomposite, and in particular, MSiTNi^{II}P nanocomposite was the most active one. The higher efficiency of MTNi^{II}P in photodegridation of MB can be attributed to the better potential match of MSiTNi^{II}P with CB of TiO_2 [42]. The result showed that nature of metal ions in the metalloporphyrins play an important role in photocatalytic activity of the nanocomposites. It is revealed that the photodegradation of MB followed first-order kinetics. Due to the ferromagnetic behavior of the photocatalysts, their separation can be simply performed by using an external magnet. The catalysts reusability was investigated and the most desirable result was obtained for MSiTNi^{II}P nanocomposite. The results show that the MSiTMP nanocomposites can be used from visible light to degrade organic pollutants in wastewater to clean-up factories.

ACKNOWLEDGMENTS

The authors gratefully appreciate the University of Mazandaran for supports of this research.

REFERENCES

[1] H. Esmaili, A. Kotobi, S. Sheibani, F. Rashchi, Int. J. Min. Met. Mat. 25 (2018) 244.

[2] J. Singh, P. Yadav, A.K. Pal, V. Mishra, in Sensors in

Water Pollutants Monitoring: Role of Material, Springer, 2020, p. 5.
[3] M.A. Raja, V. Preethi, Int. J. Hydrogen Energ. 45 (2020) 7616.
[4] P.S. Basavarajappa, S.B. Patil, N. Ganganagappa, K.R. Reddy, A.V. Raghu, C.V. Reddy, Int. J. Hydrogen Energ. 45 (2020) 7764.
[5] D. Ma, J. Li, A. Liu, C. Chen, Materials 13 (2020) 1734.
[6] A. Zielińska-Jurek, Bielan, Z. Dudziak, S. Wolak, I. Sobczak, Z. Klimczuk, T. Hupka, J. Catal. 7 (2017) 1.
[7] A. Mishra, A. Mehta, S. Basu, J. Environ. Chem. Engin. 6 (2018) 6088.
[8] S. Kanan, M.A. Moyet, R.B. Arthur, H.H. Patterson, Catal. Rev. 62 (2020) 1.
[9] F. Chang, H. Chen, X. Zhang, B. Lei, X. Hu, Sep. Purif. Technol. 238 (2020) 116442.
[10] T. Xu, P. Wang, D. Wang, K. Zhao, M. Wei, X. Liu, H. Liu, J. Cao, Y. Chen, H. Fan, J. Alloy Compd. 1 (2020) 155689.
[11] C. Borgohain, J. Borah, Matt. Res. Express 7 (2020) 016111.
[12] C. Liu, Y. Li, Q. Duan, Appl. Surf. Sci. 503 (2020) 144111.
[13] E. Alzahrani, Am. J. Analyt. Chem. 8 (2017) 95.
[14] A. Pourzad, H.R. Sobhi, M. Behbahani, A. Esrafili, R.R. Kalantary, M. Kermani, J. Mol. Liq. 299 (2020) 112167.
[15] R. Kaveh, M. Mokhtarifar, M. Bagherzadeh, A. Lucotti, M.V. Diamanti, M. Pedeferri, Molecules 25 (2020) 2996.
[16] L.-Y. Huang, J.-F. Huang, Y. Lei, S. Qin, J.-M. Liu, Catalysts 10 (2020) 656.
[17] Z. Li, C. Wang, Z. Su, W. Zhang, N. Wang, G. Mele, J. Li, Matter. Chem. Phys. 1 (2020) 123228.
[18] S. Gonuguntla, A. Tiwari, S. Madanaboina, G. Lingamallu, U. Pal, Int. J. Hydrogen Energ. 45 (2020) 7508.
[19] M. Gaeta, G. Sanfilippo, A. Fraix, G. Sortino, M. Barcellona, G. Oliveri Conti, M.E. Fragalà, M. Ferrante, R. Purrello, A. D'Urso, Int. J. Mol. Sci. 21 (2020) 3775.
[20] J. Niu, B. Yao, Y. Chen, C. Peng, X. Yu, J. Zhang , G. Bai, Appl. Surf. Sci. 271 (2013) 39.
[21] H. Wang, D. Zhou, Z. Wu, J. Wan, X. Zheng, L. Yu, D.L. Phillips, Mater. Res. Bull. 57 (2014) 311.
[22] M. Rabbani, M. Heidari-Golafzani, R. Rahimi, Matter. Chem. Phys. 179 (2016) 35.
[23] X. Zhao, X. Liu, M. Yu, C. Wang, J. Li, Dyes. Pig. 136 (2017) 648.
[24] X.-F. Lü, H. Qian, G. Mele, A. De Riccardis, R. Zhao, J. Chen, H. Wu , N.-J. Hu, Catl. Today 281 (2017) 45.
[25] D. Larowska, J.M. O'Brien, M.O. Senge, G. Burdzinski, B. Marciniak, A. Lewandowska-Andralojc, J. Phys. Chem. C 1 (2020) 1.
[26] H.P. Mota, R.F. Quadrado, B.A. Iglesias, A.R. Fajardo, Appl. Catal. B. Env. 1 (2020) 119208.
[27] C. Huang, Y. Lv, Q. Zhou, S. Kang, X. Li, J. Mu, Ceram. Int. 40 (2014) 7093.
[28] J.P. Ghosh, C.H. Langford, G. Achari, J. Phys. Chem. A 112 (2008) 10310.
[29] C. Casado, R. Timmers, A. Sergejevs, C. Clarke, D. Allsopp, C. Bowen, R. van Grieken, J. Marugán, Chem. Eng. J. 327 (2017) 1043.
[30] N. Doss, G. Carré, V. Keller, P. André, N. Keller, Water, Air, Soil Pollut. 229 (2018) 1.
[31] L. Qiu, A. Dong, S. Zhang, S. Wang, Z. Chang, Y. Lu, Z. Sui, L. Feng, Q. Chen, J. Mater. Sci. 1 (2020) 1.
[32] T.A. Gad-Allah, S. Kato, S. Satokawa, T. Kojima, Desalination 244 (2009) 1.
[33] A. Jesus, J. Jesus, R. Lima, K. Moura, J. Almeida, J. Duque, C. Meneses, Ceram. Int. 46 (2020) 11149.
[34] V.D. Rumyantseva, A.S. Gorshkova, A.F. Mironov, Macroheterocycles 6 (2013) 59.
[35] A.D. Adler, F.R. Longo, J.D. Finarelli, J. Goldmacher, J. Assour, L. Korsakoff, J. Org. Chem. 32 (1967) 476.
[36] A. Monshi, M.R. Foroughi, M.R. Monshi, WJNSE 2 (2012) 154.
[37] D.J. Lim, N.A. Marks, M.R. Rowles, Carbon 162 (2020) 475.
[38] D. Bu, N. Li, Y. Zhou, H. Feng, F. Yu, C. Cheng, M. Li, L. Xiao, Y. Ao, N. J. Chem. 2012 (2020) 1.
[39] P. Makuła, M. Pacia, W. Macyk, J. Phys. Chem. Lett. 9 (2018) 6814.
[40] M. Wei, J. Wan, Z. Hu, Z. Peng, B. Wang, J. Mater. Sci.: Mater. Elec. 27 (2016) 4026.

[41] O. Bajjou, A. Bakour, M. Khenfouch, M. Baitoul, B. Mothudi, M. Maaza, E. Faulques, J. Mater. Sci.: Mater. Elec. 29 (2018) 8594.
[42] W.-J. Sun, J. Li, G.-P. Yao, F.-X. Zhang, J.-L. Wang, Appl. Surf. Sci. 258 (2011) 940.
[43] G. Mele, R. Del Sole, G. Vasapollo, E. García-López, L. Palmisano, L. Jun, R. Słota, G. Dyrda, Res. Chem. Intermed. 33 (2007) 433.
[44] D. Wang, J. Yang, X. Li, J. Wang, H. Zhai, J. Lang, H. Song, Phys. Status Solidi A 214 (2017) 1.
[45] F. Bavarsiha, M. Rajabi, M. Montazeri-Pour, J. Mater. Sci.: Mater. Elec. 29 (2018) 1877.
[46] H. Ghafuri, M. Dehghani, A. Rashidizadeh, M. Rabbani, Optik 179 (2019) 646.
[47] C.-F. Chang, C.-Y. Man, Colloids Surf., A: Phys. Chem. Eng. Asp. 441 (2014) 255.
[48] X.-F. Lü, W.-J. Sun, J. Li, W.-X. Xu, F.-X. Zhang, Spectrochim. Acta. A. Mol. Biomol. Spectrosc. 111 (2013) 161.
[49] V. Augugliaro, M. Bellardita, V. Loddo, G. Palmisano, L. Palmisano, S. Yurdakal, J. Photo. Chem. Photo. Bio. C 13 (2012) 224.
[50] Q. Mu, Y. Sun, A. Guo, X. Yu, X. Xu, A. Cai, X. Wang, Matt. Res. Express 6 (2019) 1.
[51] C.Y. Lee, J.T. Hupp, Langmuir 26 (2009) 3760.